Al-Azhar Bull. Sci. Vol. 24, No. 2 (Dec.): pp. 53-64, 2013.

CRYSTAL TO AMORPHOUS TRANSITION OF SI AND AR IMPLANTED SILICON USING SINGLE-EFFECTIVE OSCILLATOR MODEL

M. A. EL-SHERBINY

Physics Department, Faculty of Science, Al-Azhar University, Cairo 11884, Egypt
e. mail: sherbinypsi@yahoo.com

Abstract

Complex dielectric function was used to calculate refractive index and optical dispersion parameters for silicon wafers <100> implanted with Si and Ar ions with different fluences. Energies of 200 and 800 keV were used, in order to relate ion implantation parameters with lattice perturbation. Single-effective oscillator energy, average strength of the interband optical transition, zero frequency (static) refractive index, moments of ε(E) dispersion spectra, plasma angular frequency, lattice energy, the contribution of the free carriers and Urbach energy were obtained on the basis of the single-effective oscillator model proposed by Wemple and DiDomenico to monitor crystalline-amorphous transformation.

Used experimental techniques and damage profiles have been demonstrated elsewhere[(1)]. Real and imaginary parts of the dielectric constant were calculated from the recently measured ellipsometric parameters (phase difference Δ and amplitude ratio ψ) [(1,2).]

Progressive increase in the absorption coefficient magnitude below fundamental edge, oscillator energy E_0, and oscillator average strength E_d with increasing ion fluence is primarily a defect formation effect, which produce a perturbation to the periodic potential of the crystal resulting a localized states in the band gap. The suggested mechanism can account for the decrease of both lattice energy (E_l) and N/m^* behavior. Decrease of static refractive index in the low fluencies interpreted as a decrease in the dangling bonds which attributed to restructuring of the bonds. With increase of fluence the dangling bonds increased denoting formation of clusters together and increasing its mean size up to a percolation threshold. Increasing Urbach energy as a function of fluencies was observed and interpreted from the point view of Mott–Anderson transition.

Keywords:

Ion implantation, lattice perturbation, Crystal to amorphous transition**,** Wemple and DiDomenico, Single-effective oscillator energy, Dispersion energy, Plasma frequency, moments of dispersion spectra.

1- Introduction:

Ellipsometry is a powerful, nondestructive technique for determining the complex dielectric function of thin film as well as obtaining information regarding the band structure, critical points, interfaces and the semiconductor alloy composition. This technique was used extensively to monitor changes in optical properties in manner to study damage in semiconductors induced by implantation with low and medium energy ions. Literatures were suggested two models for amorphization, The first thought that amorphization is a phase transition induced by accumulation of sufficient number of defects in crystalline Silicon known as the homogeneous amorphization model[(3)]. The second is the heterogeneous amorphization which thought that amorphous layer can be formed due to sufficient overlap of the

amorphized cylindrical cascades. More recently, the defect induced nucleation and growth of amorphous Si (a-Si). This has been proposed to get a view to comprehend different aspects of the homogeneous amorphization model[4].

The effect of irradiation fluence on the optical spectra of silicon wafers <100> implanted with Si and Ar ions with different fluencies, at energies 200 and 800 keV respectively were studied in earlier work[1, 2]. The spectral range was chosen above the fundamental absorption edge and below the first direct transition which assigned as E_2 transition at 4.27 eV from $X_1 \rightarrow X_4$, E'_0 transition at 3.287 eV from $\Gamma_{15} \rightarrow \Gamma'_{25}$ and transition E_1 at 3.437 eV from $\Lambda^v_3 \rightarrow \Gamma^c_1$. The ellipsometric parameters (phase difference Δ and amplitude ratio ψ) were used to calculate the dielectric function to identify the higher order electronic transitions in the Brillouin zone of crystalline-amorphous (c-a) silicon interfaces under ion implantation. In this interpretation thr variation of the interband critical point parameters (CPs) with fluence (Φ) was used to monitor crystalline-amorphous transformation[2]. The present work aims to relate ion implantation and lattice perturbation, which is relatively less examined[5-9]. However, dielectric function data for Silicon and Argon implanted silicon extracted from this evaluation was used to calculate the optical constants, real and imaginary parts of refractive index, which have a considerable importance for applications in integrated optical devices.

2- Calculation technique:

Complex dielectric function is known to describe the optical properties of a medium at all photon energies and given by

$$\varepsilon(\lambda) = \varepsilon_1(\lambda) + i.\ \varepsilon_2(\lambda)$$

where ε_1 is the volume polarization term for induced dipoles and ε_2 is the volume absorption related to carrier concentration. Using the complex dielectric function obtained from elleipsometry, it is possible to calculate the refractive index (n) and extinction coefficient (k), which are the important parameters to be considered when designing optoelectronic devices[4].

Real and imaginary parts of refractive index were calculated using the relation

$$n = \frac{1}{\sqrt{2}}\left(\varepsilon_1 + \left(\varepsilon_1^2 + \varepsilon_2^2\right)^{1/2} \right)^{1/2}$$

$$k = \frac{1}{\sqrt{2}}\left(-\varepsilon_1 + \left(\varepsilon_1^2 + \varepsilon_2^2\right)^{1/2} \right)^{1/2}$$

Where ε_1 and ε_2 are real and imaginary parts of the dielectric constant. Absorption coefficient calculated from the expression $\alpha = \frac{4\pi k}{\lambda}$ where k is the extinction coefficient and λ is the wavelength of incident photon. According to the single-

effective oscillator model proposed by Wemple and DiDomenico[10] the optical data can be described to an excellent approximation by the relation:

$$n^2 = 1 + \frac{E_d\, E_0}{E_0^2 - E^2}$$

Where E_0 is the single-effective oscillator energy, E_d is the dispersion energy which is a measure of the average strength of the inter-band optical transitions which is related to the coordination number of given atom and E is the photon energy. This dispersion plays an important role in the research for optical materials, because it is a significant factor in optical communication and in designing devices for spectral dispersion. According to this model, the interband transitions can be approximated by individual oscillator and summation over oscillators can be approximated by a summation of the first strong oscillator and a proper combination of the higher order contributions providing a single effective oscillator model. This model describes the dielectric response for transitions below the optical gap and plays an important role in determining the behavior of the refractive index[11].

The parameters of the single oscillator model E_0 and E_d are connected to the zero frequency (static) refractive index n_0 and the moments (M_{-1}, M_{-3}) of ε(E) dispersion spectrum which can be estimated through the relations[12]

$$n_0^2 = 1 + \frac{E_d}{E_0}$$

$$E_0^2 = \frac{M_{-1}}{M_{-3}}$$

$$E_d^2 = \frac{M_{-1}^3}{M_{-3}}$$

Plasma angular frequency ω_P can be expressed as

$$\omega_P = \sqrt{\frac{N e^2}{m^* \varepsilon_{Si}}}$$

where N is the majority carrier density, e is the elemental charge, m^* is the effective mass of the carriers and ε_{Si} is the dielectric constant of silicon. On the other hand the refractive index can be linked to the resonance frequency and the volume plasma frequency according to the relation $n_0 = n(\omega \to 0) = 1 - \frac{\omega_P^2}{\omega_0^2}$, which suggests that n_0 is imaginary for $\omega_0 \prec \omega_P$ [13, 14].

At long wavelength where $E^2 \prec\prec E_0^2$ the lattice contribution given by[15]

$$n^2 - 1 = E_d / E_0 - E_l^2 / E^2$$

Where E_l is the lattice energy. A plot of n^2-1 versus $1/E^2$ approaches a straight line, the intercept is the ratio E_d / E_0 , and the slope is $-E_l^2$, thus the values of the lattice energy E_l can be obtained.

To describe the contribution of the free carriers the following relation[16] was used

$$\varepsilon = n^2 = \varepsilon_\infty - \left(\frac{e^2}{4\pi c^2 \varepsilon_0} \right) \left(\frac{N}{m^*} \right) \lambda^2$$

where c is the velocity of light, ε_0 the permittivity of free space, ε_∞ is the high frequency dielectric constant, e is the elementary charge, N is the free carrier concentration and m^* is the effective mass of the charge carriers.

In the case of non-crystalline materials there can be less dense localized energy states, near the valence (HOMO) and conduction (LUMO) band edges, known as "Urbach energy bands"[17].

The exponential dependence of the absorption coefficient on photon Energy takes the form

$$\alpha = \alpha_0 \exp\left(\frac{h\nu}{E_U} \right)$$

Where α_0 is the pre-exponential factor, ν is the frequency of radiation, h is Planck's constant, and E_U is the Urbach energy which is the width of the localized states associated with dangling bonds or similar defects and extends into the forbidden gap[18,19]. Taking the natural logarithm of this equation gives

$$\ln \alpha = \ln \alpha_0 + \frac{h\nu}{E_U}$$

By plotting $\ln \alpha$ against photon energy in the range (10^3 – 10^4 cm), the Urbach energy can be determined directly from the reciprocal of the slopes of the linear portion of these curves, This region is attributed to the electronic transition between a localized band tail. The origin of E_U is related to the thermal vibrations in the lattice.

3- Results and discussion:

Absorption coefficient (α), real and imaginary parts of the dielectric constant and all other parameters were calculated using the procedure in section (2) from recently

measured ellipsometric parameters (phase difference Δ and amplitude ratio ψ)[1,2]. Figure (1) shows the dependence of the absorption coefficient on photon energy in the range 1.7 to 3.4 eV. The choice of the considered range is that it contains the two absorption regions, the first region from 1.7 to 2.9 eV arises from absorption via Si dangling bond defect states in the middle of the band-gap, the second from 2.9 to 3.4 eV is related to absorption involving band tail states.

It is clear from the figure that the absorption edge exhibits red shift and shows pronounced broadening as the fluence of Si increases. Furthermore, a progressive increase in the absorption coefficient magnitude below fundamental edge with increasing ion fluence is usually attributed to the increased carrier concentration, induced by increasing defect level in the band gap.

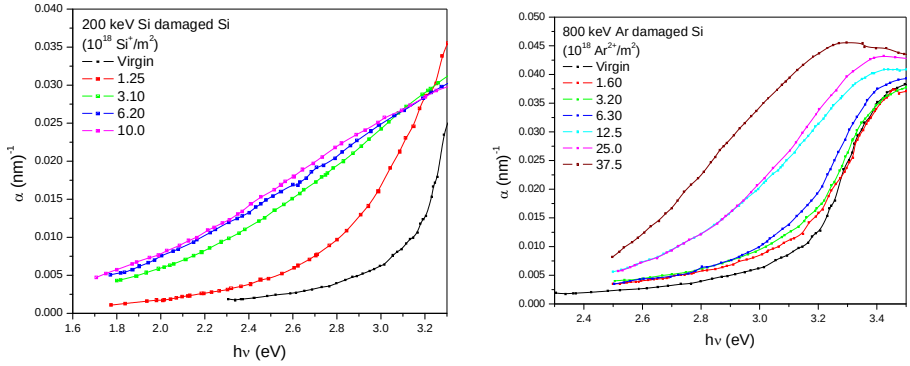

Figure (1): Absorption coefficient $\alpha(nm^{-1})$ as a function of incident energy *hν(eV)*.

By plotting E^2 against $1/(n^2 - 1)$ the values of E_0 and E_d can be estimated. The data was fitted to the best straight line as shown in figure (2)

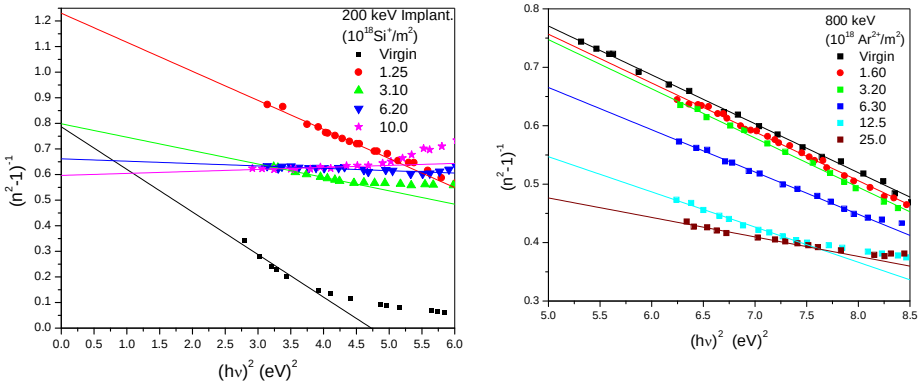

Figure (2): Linear fit for $(n^2–1)^{-1}$ versus photon energy squared by the Wemple DiDomenico for Si and Ar damaged Si at different ion fluence.

The estimated values of n_0, E_0 and E_d together with their moments M_{-1} and M_{-3} for the virgin and as implanted silicon with deferent fluencies are given in tables (1,2) for silicon and Argon respectively , where $n_0 = \sqrt{\varepsilon_0}$.

The obtained values show an increase in the oscillator energy and the average strength with increasing disorder of the sample. The increase in oscillator average strength could be attributed to the increase of the average coordination number of the atoms. The lowest energy oscillator strength is the largest contributor to n, which agrees with the results of Hamide et. Al[20].

Table (1): Fluence dependence of plasma frequency ω_P, static refractive index, dispersion oscillator energy (E_0), Average strength of the interband optical transition (E_d), lattice energy (E_l), the ratio of free carrier concentration to the free carrier effective mass N/m^* and moments of ε(E) dispersion spectrum for 200 keV Si damaged Si. (All tabulated energies are in eV)

Fluence (10^{18} Si^+/m^2)	ω_P (eV)	n_0	oscillator energy E_0	Average strength E_d	Lattice energy E_l	N/m^*	M_{-1}	M_{-3}
Virgin	4.362	1.507	2.174	2.764	4.504	08.619	1.128	0.239
1.25	3.933	1.346	3.291	2.675	4.758	14.455	0.901	0.083
3.10	3.867	1.500	3.904	4.891	2.107	05.334	1.119	0.073
6.20	3.829	1.584	8.443	12.762	1.674	03.895	1.229	0.017
10.0	3.812	1.635	8.734	14.639	1.596	04.139	1.294	0.017

Table (2): Fluence dependence of plasma frequency ω_P, static refractive index, dispersion oscillator energy (E_0), Average strength of the interband optical transition (E_d), lattice energy (E_l), the ratio of free carrier concentration to the free carrier effective mass N/m^* and moments of ε(E) dispersion spectrum for 800 keV Ar damaged Si. (All tabulated energies are in eV)

Dose (10^{18} Ar^{2+}/m^2)	ω_P (eV)	n_0	oscillator energy E_0	Average strength E_d	Lattice energy E_l	N/m^*	M_{-1}	M_{-3}
Virgin	4.362	1.507	2.174	2.764	4.504	8.619	1.128	0.239
1.60	4.140	1.361	3.749	3.191	4.620	10.700	0.923	0.066
3.20	4.091	1.362	3.725	3.188	4.821	12.386	0.925	0.067
6.30	4.000	1.405	3.769	3.670	4.357	11.257	0.987	0.069
12.5	3.837	1.476	3.753	4.426	4.305	13.057	1.086	0.077
25.0	3.722	1.598	4.392	6.829	3.999	11.956	1.247	0.064

On the basis of the above mentioned model, the single oscillator energy E_0 increases from 2.174 eV for the virgin sample to 8.735 eV for the sample implanted with $10^{18}\ Ar^{2+}/m^2$ and the oscillator average strength E_d increases from 2.764 to

14.64 eV for the same samples. The observed increase in E_d with ion fluence is primarily a defect formation effect. Such defects produce a perturbation to the periodic potential of the crystal resulting a localized states in the band gap which increase with increasing ion fluence.

Figure (3) shows the variation of the ratio of free carrier concentration to the free carrier effective mass N/m^* and lattice dielectric constant as a function of ion fluence. A sharp increase can be noticed clearly for the sample with fluence 1.25x 10^{18} Si^+/m^2 followed by a sharp decrease for the higher disordered sample till it saturates. In the case of Ar damaged Si, sharp increase noticed up to the fluence 3.2 x 10^{18} Ar^{2+}/m^2 followed by no appreciable difference above these fluencies indicating saturation in the carrier compensation above the threshold of amorphization, and this may indicate no change in the microstructure beyond the amorphization threshold, except for an increase in the thickness of the amorphous layer with higher fluencies. At low fluence, the incident energy causes low defect concentration, which most likely point defects. The density of such defects increases by increasing ion fluence gradually, and ultimately the amorphous state is achieved. This suggested mechanism can account for the decrease of both lattice energy (E_l) and N/m^* behavior. It is clearly observed that the dependence of both E_l and N/m^* is different in case of Ar from that observed for Si. This is most likely due to the difference in atomic weight and volume of the implanted ion species (weigh of 39.948 amu for Argon and 28.0855 amu for Silicon, volume is 24.2 cm^3 mol^{-1} for Ar and 11.6 cm^3 mol^{-1} for Si) which cause changes in bond length.

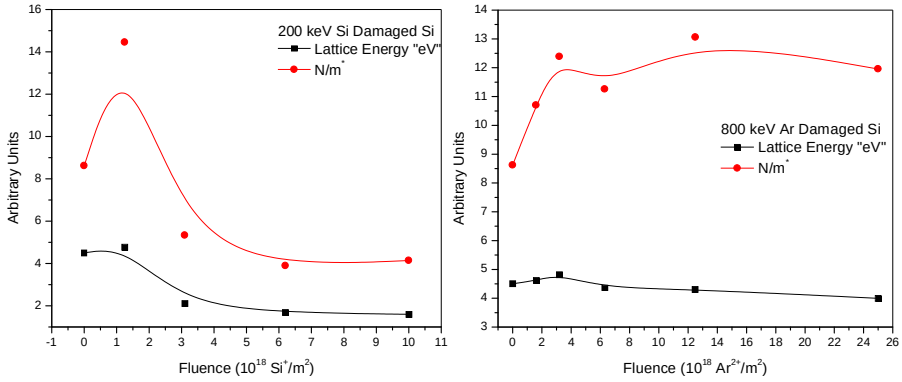

Figure (3): Lattice energy *E1* and ratio of free carrier concentration to the free carrier effective mass *N/m as a function of implanted Si and Ar ion concentrations.**

Figure (4) presents the dependence of moment of dispersion spectra M_{-1} and M_{-3}, Static refractive index n_0 and plasma frequency ω_p on the fluence of both Si and Ar ions, virgin and as implanted samples. All considered parameters follow one common behavior where they decrease up to 1.25 x 10^{18} Si^+/m^2 and 2 x 10^{18} Ar^{2+}/m^2. Static refractive index gives an information about the dangling bonds in the

samples, the decrease in the low fluencies may indicates a decrease in the dangling bonds which may be attributed to restructuring of the bonds up to a percolation threshold. With increase of fluence the dangling bonds increased denoting formation of clusters together and increasing the mean cluster size. Continuous decrease in plasma frequency indicates disorder increase.

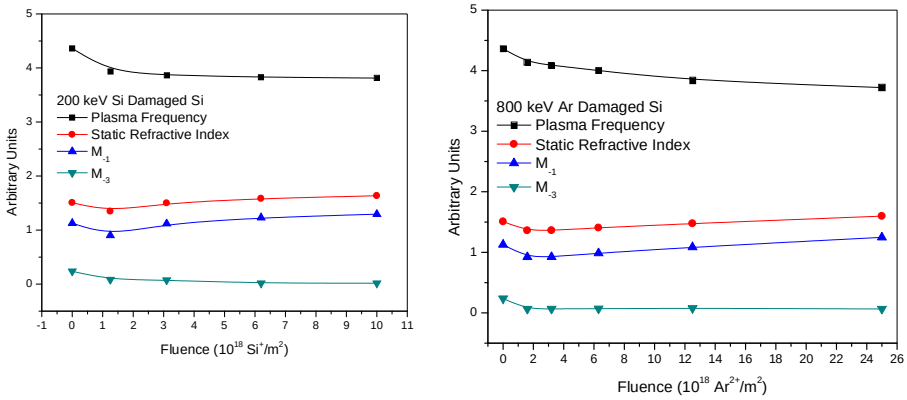

Figure (4): Dependence of moment of dispersion spectra M_{-1} and M_{-3}, Static refractive index n_0 and plasma frequency ω_p on the fluence for both Si and Ar ions, virgin and as implanted samples.

The plot of E_d and E_0 obtained using Wemple and DiDomenico relation as a function of ion fluence are shown in figure (5). The figure reveals that E_d remains nearly constant at the low fluence and increases rapidly with further increase of fluence, this may indicate the changes in the characteristics of the electronic transition from the valence to conduction band of the damaged substrates. E_0, however, increases with increasing fluence and tends to saturate up of certain fluence. E_0 is related to the structural disorder. Crystalline to amorphous transition and subsequent microstructural evolution in silicon induced by Ar^+ ion implantation over a wide range of ion fluences ($6x10^{13}$ –$1x10^{17}$ cm^{-2}) with 120 keV energy have been investigated by Giri et. Al.,[4]. They found that E_0 and E_d decrease substantially at fluences above the amorphization threshold. Below the amorphization threshold, no substantial change in these parameters is observed indicating the insensitivity of these parameters to the presence of point defects, despite a high concentration being present in the damaged Si, in contrast to this work.

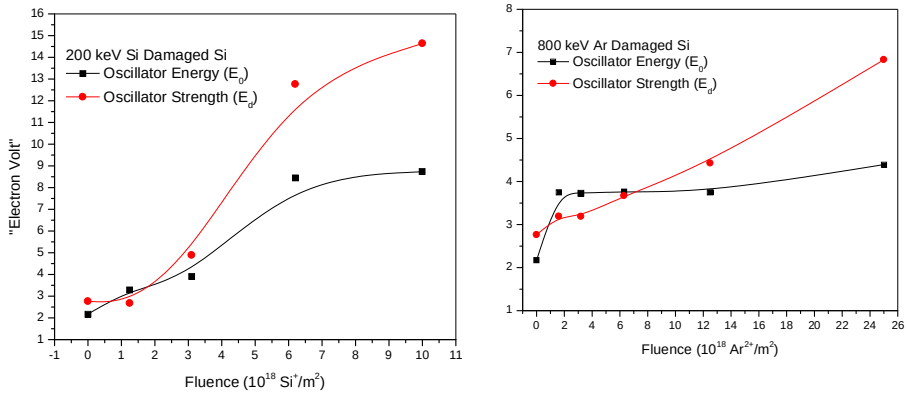

Figure (5): Optical oscillator strength (E_d) and oscillator energy (E_0) as a function of fluence for crystalline and as implanted Si and Ar ions

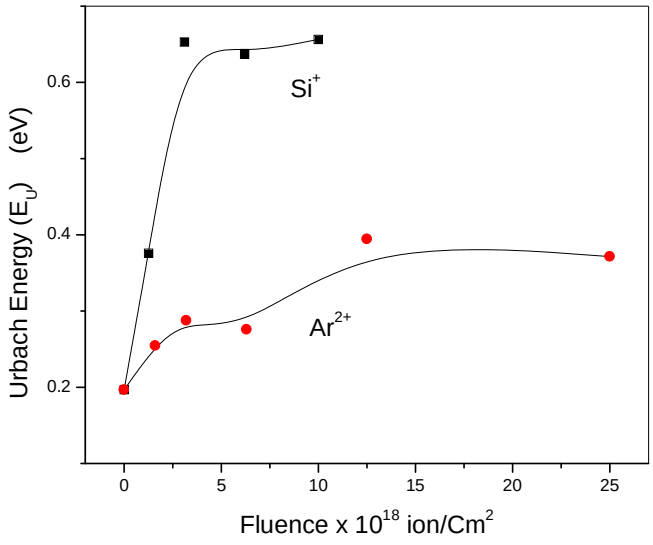

Figure (6): Urbach energy as a function of fluencies for both Si and Ar damage Silicon.

Figure (6) represents the Urbach energy as a function of fluencies for both Si and Ar damage Silicon. Higher values indicate higher structural disorder. These results may be interpreted from the point view of Mott – Anderson transition[21]. At low fluencies where the long range order still present, impurities are still ordered and may be presented as point defects in the crystal lattice, but the depth of the potential

wells is random and there are extended and localized states separated by the mobility edges. These results in increasing lattice energy and hence the ratio of free carriers to its effective mass up to certain ion fluence concentration as is clear from figure (3). With increasing ion fluence, the degree of disorder increases and nearest neighbors can overlap and localized states appear in the band gap, and the Fermi level moves towards the extended states, as we approach the percolation threshold, several clusters come together and the mean cluster size increases, and the ratio of free carriers to the effective mass decreases as a result of these localized levels which can be accounted for the variations of plasma frequency with fluence presented in figure (4). These results agree with the abrupt increase in both energy and strength of the oscillator after certain fluence level which is related to increasing the coordination number of the atoms.

Acknowledgements

The author is grateful to J. Gyulai and T. Lohner from the Research Institute for Material Science, Budapest, Hungary, for supplying them with ellipsometric data.

References

1. T. Lohner, M.A. El-Sherbiny, N.Q. Khanh, M. Fried, H. Wormeester, J. Gyulai, in: J.S. Williames, R.G. Elliman, M.C. Ridgway (Eds.), Ion Beam Modification of Materials, Elservier, Amsterdam, (1996) 797-801.
2. M.A. El-Sherbiny, H.H. El-Bahnasawy, M.M. El-Ocker, Nucl. Instr. and Meth. in Phys. Res. B 168 (2000) 510 – 520.
3. M.O. Ruault, J. Chaumont, H. Bernas, Nucl. Instrum. Methods Phys. Res. 209-210 part 1, (1983) 351 - 356.
4. P.K. Giri, S. Tripurasundari, G. Raghavan, B.K. Panigrahi, P. Magudapathy, K.G.M. Nair, A.K. Tyagi, J. Appl. Phys., Vol. 90, No. 2, 15 July (2001), 659 – 669.
5. Y.Z. Hu, J.W. Andrews, M. Li, E.A. Irene, Nucl. Instr. and Meth. B 59–60 (1991) 76.
6. N.V. Nguyen, K. Vedam, J. Appl. Phys. 67 (1990) 3555.
7. R.W. Collins, B.G. Yacobi, K.M. Jones, Y.S. Tsuo, J. Vac.Sci. Technol. A 4 (1986) 153.
8. A. Borghesi, A. Paggi, A. Stella, G. Guizzetti, D. Bisero, G. Queirolo, J. Appl. Phys. 67 (11) (1990) 7045.
9. S. Tripura Sundari, Nucl. Instr. Meth. in Phys. Res. B 215 (2004) 157–161.
10. S. H. Wemple, M. DiDomenico, J. Phys. Rev. Lett. 23, 1156 (1969).
11. M.A. Gaffara, A. Abu El-Fadlb, S. Bin Anooz, Physica B 327 (2003) 43–54.
12. K. Goksen, N.M. Gasanly, H. Ozkan, ACTA PHYSICA POLONICA A, No.1, Vol.112 (2007), 93-100.
13. S. H. Wemple, M. Di Domenico, Phys. Rev., **B3,** 1338 (1971).
14. S. H. Wemple, Phys. Rev., **B7,** 3767 (1973).

15. S.Y. El-Zaiat, M.B.El-Den,S.U.El-Kameesy,Y.A.El-Gammam, Optics & Laser Technology 44 (2012) 1270–1276.
16. M.M. El-Nahass, S. Yaghmour, Applied Surface Science 255 (2008) 1631– 1636.
17. Somik Banerjee, A. Kumar, Nucl. Instr. and Meth. in Phys. Res. B 269 (2011) 2798–2806.
18. C. I. Oriaku, J. C. Osuwa, C. H. Njoku , Journal of Non-Oxide Glasses, Vol. 3, No 1, 2011, p. 25-30.
19. S.H. Rejeb, R. Gharbi, M. Fathallaha, F. Demichelis, C.F. Pirri, E. Tresso, G. Crovini, Optical Materials 6 (1996) 13-16.
20. Hamide Kavak, Sltk Eker, Amirullah Mamedov, Journal of Quantitative Spectroscopy & Radiative Transfer 86 (2004) 223–229.
21. D. C. Tsui, S. J. Allen, J. Physical Review Letters 32 (1974) 1200 – 1202.